

# Semi-classical description of electron dynamics in extended systems under intense laser fields

Mizuki Tani,<sup>1,2,\*</sup> Tomohito Otobe,<sup>2,†</sup> Yasushi Shinohara,<sup>1,3</sup> and Kenichi L. Ishikawa<sup>1,3,4,‡</sup>

<sup>1</sup>*Department of Nuclear Engineering and Management,  
Graduate School of Engineering, The University of Tokyo,  
7-3-1 Hongo, Bunkyo-ku, Tokyo 113-8656, Japan*

<sup>2</sup>*Kansai Photon Science Institute, National Institutes for Quantum  
and Radiological Science and Technology (QST), Kyoto 619-0215, Japan*

<sup>3</sup>*Photon Science Center, Graduate School of Engineering,  
The University of Tokyo, 7-3-1 Hongo, Bunkyo-ku, Tokyo 113-8656, Japan*

<sup>4</sup>*Research Institute for Photon Science and Laser Technology The University of Tokyo,  
7-3-1 Hongo, Bunkyo-ku, Tokyo 113-0033, Japan*

(Dated: February 10, 2022)

We propose a semi-classical approach based on the Vlasov equation to describe the time-dependent electronic dynamics in a bulk simple metal under an ultrashort intense laser pulse. We include in the effective potential not only the ionic Coulomb potential and mean-field electronic Coulomb potential from the one-body electron distribution but also the exchange-correlation potential within the local density approximation (LDA). The initial ground state is obtained by the Thomas-Fermi model. To numerically solve the Vlasov equation, we extend the pseudo-particle method, previously used for nuclei and atomic clusters, to solids, taking the periodic boundary condition into account. We apply the present implementation to a bulk aluminum (FCC) conventional unit cell irradiated with a short laser pulse. The optical conductivity, refractive index, extinction coefficient, and reflectivity as well as energy absorption calculated with the Vlasov-LDA method are in excellent agreement with the results by the time-dependent density functional theory and experimental references.

PACS numbers: Valid PACS appear here

## I. INTRODUCTION

The interaction of ultrashort (fs-ps) intense laser pulses with solids is relevant to a wide area of research ranging from high-harmonic generation [1–5] to material machining [6–14]. The process of ultrafast laser micromachining, which can suppress heat-affected zone, starts from the energy transfer from the laser to the material by electron excitation, followed by that from the hot electrons to the lattice. As a result, the material undergoes phase and/or structural transition[15], leaving a change of the optical constants or a defect behind [16], which eventually leads to ablation, drilling, or structuring [17–32].

The comprehensive modeling of laser material machining is highly complex, multi-scale in both time and space, multi-phase (solid, fluid, plasma, cluster, etc.), and possibly accompanied by chemical reactions. Plasma or continuum models [6, 8, 33–36], for example, have been employed to describe and simulate such processes, advancing understanding. However, they have difficulties in examining initial transient dynamics before the local thermodynamic equilibrium is reached.

It has now become possible to describe the attosecond-femtosecond electron dynamics under intense laser fields with the time-dependent density-functional the-

ory (TDDFT) [37–40] or time-dependent density-matrix methods [41–43]. TDDFT is an *ab initio* method that offers a good compromise between accuracy and computational feasibility. Its computational cost is, however, still very high, especially, if one wants to perform long-timescale simulation, coupling it with molecular dynamics and electromagnetic-field analysis.

In TDDFT, each electron orbital satisfies the time-dependent Kohn-Sham (TDKS) equation [see Eq. (1) below]. The leading order of a semiclassical  $\hbar$  expansion of the TDKS equation reduces to the Vlasov equation, which describes the temporal evolution of the electron distribution function in phase space. Thus, Vlasov-based approaches are expected to be a cost-effective alternative to TDDFT, in particular, for metals. Such approaches have previously been applied to ionization and explosion dynamics of molecules [44, 45] and metal clusters [46–51]. The Vlasov equation is numerically solved with so-called pseudo-particle methods in these studies, which represent the electron cloud as an assembly of classical test particles whose motion is governed by Newton's equations of motion. There are several reports of application to Na clusters, well agreeing with TDDFT results [49–53].

In this paper, we extend the pseudo-particle method based on the Vlasov equation to the description of electron dynamics in extended systems under intense laser fields. The effective potential acting on the electrons contains not only the ionic potential, interelectronic Hartree potential, and interaction with laser but also the exchange-correlation potential within the local-

\* mzktani@atto.t.u-tokyo.ac.jp

† corresponding author: otobe.tomohito@qst.go.jp

‡ corresponding author: ishiken@n.t.u-tokyo.ac.jp

density approximation (LDA), and incorporates the periodic boundary condition. We apply the present method to bulk aluminum. The calculated optical conductivity, refractive index, extinction coefficient, and reflectivity as well as energy absorption are in excellent agreement with TDDFT calculations and experimental references.

The present paper is organized as follows. Section II describes our simulation methods. We review the Vlasov equation and describe our numerical implementations with the periodic boundary condition. In Sec. III we describe numerical application to bulk aluminum and compare the results with TDDFT and measurement values. The conclusions are given in Sec. IV.

## II. METHODS

### A. Vlasov equation

Among the methods for treating quantum many-body dynamics, TDDFT provides a feasible computational framework for treating electronic systems' optical response or charged particles' collision phenomena [54]. The time propagation of a  $N_e$ -electron system comes down to solving a set of equations for the Kohn-Sham orbitals  $\{\phi_i(\mathbf{r}, t)\}$  that evolve in a self-consistent mean field [55],

$$i\hbar \frac{\partial}{\partial t} \phi_i(\mathbf{r}, t) = h_{\text{KS}}[n_e(\mathbf{r}, t)] \phi_i(\mathbf{r}, t), \quad (1)$$

where,

$$h_{\text{KS}}[n_e(\mathbf{r}, t)] = -\frac{\hbar^2}{2m} \nabla^2 + V_{\text{eff}}[n_e(\mathbf{r}, t)], \quad (2)$$

denotes the Kohn-Sham Hamiltonian,  $m$  the electron mass,  $V_{\text{eff}}$  the effective potential (see below), and the time-dependent electron density  $n_e(\mathbf{r}, t)$  is defined as,

$$n_e(\mathbf{r}, t) = \sum_{i=1}^{N_e} |\phi_i(\mathbf{r}, t)|^2. \quad (3)$$

Analogously, the density operator  $\hat{\rho}(t)$  is defined as,

$$\langle \mathbf{r} | \hat{\rho}(t) | \mathbf{r}' \rangle = \sum_{i=1}^{N_e} \phi_i^*(\mathbf{r}, t) \phi_i(\mathbf{r}', t), \quad (4)$$

whose evolution is governed by the von-Neumann equation (vNE),

$$\frac{\partial}{\partial t} \hat{\rho}(t) = -\frac{i}{\hbar} [\hat{h}_{\text{KS}}(t), \hat{\rho}(t)]. \quad (5)$$

Performing the Wigner transformation [56] and taking the limit  $\hbar \rightarrow 0$ , the density operator  $\hat{\rho}(t)$  is mapped onto a real function  $f(\mathbf{r}, \mathbf{p}, t)$ , which obeys the Vlasov

equation,

$$\begin{aligned} \frac{\partial}{\partial t} f(\mathbf{r}, \mathbf{p}, t) \\ = -\frac{\mathbf{p}}{m} \cdot \nabla_{\mathbf{r}} f(\mathbf{r}, \mathbf{p}, t) + \nabla_{\mathbf{r}} V_{\text{eff}}[n_e(\mathbf{r}, t)] \cdot \nabla_{\mathbf{p}} f(\mathbf{r}, \mathbf{p}, t), \end{aligned} \quad (6)$$

which is a classical alternative to the vNE, Eq. (5), where  $\mathbf{p}$  is the electron canonical momentum. Here,  $f(\mathbf{r}, \mathbf{p}, t)$  is interpreted as the electron distribution in phase space.

The effective potential  $V_{\text{eff}}$  is a functional of the electron density distribution  $n_e(\mathbf{r}, t)$  and decomposed into,

$$V_{\text{eff}}[n_e(\mathbf{r}, t)] = V_{\text{Coulomb}}[n_e(\mathbf{r}, t)] + V_{\text{xc}}[n_e(\mathbf{r}, t)] + V_{\text{ext}}(\mathbf{r}, t), \quad (7)$$

with the exchange-correlation potential  $V_{\text{xc}}$ , external field potential  $V_{\text{ext}}$ , and,

$$V_{\text{Coulomb}}[n_e(\mathbf{r}, t)] = \sum_i V_{\text{ps}}(\mathbf{r} - \mathbf{r}_i) + V_{\text{H}}[n_e(\mathbf{r}, t)], \quad (8)$$

where  $i$ ,  $V_{\text{ps}}$  and  $V_{\text{H}}$  denote the label of ions and the spherically symmetric ionic pseudopotential and the electron-electron Hartree potential, respectively.

Several previous works for Na clusters have used their original pseudo potentials [46, 47], adjusted so that the simulation results reproduce the static and dynamical properties of the system. In this work, instead, we employ the modified Heine-Abarenkov type local pseudo potential for  $V_{\text{ps}}$ ,

$$V_{\text{ps}}(r) = -\frac{z}{R} e \left\{ \frac{1}{r} [1 - (1 + \beta r) e^{-\alpha r} - A e^{-r}] \right\} (r = |\mathbf{r}|), \quad (9)$$

where  $z$  is the number of the valence electrons, and  $A, R, \alpha$ , and  $\beta$  are material dependent parameters determined by *ab initio* density functional formalism in Ref. [57], thus, independently from Vlasov simulations. Their values for the bulk aluminum crystal are  $A = 3.574$  a.u.,  $\alpha = 3.635$  a.u.,  $\beta = 0.8343$  a.u.,  $R = 0.334$  a.u.,  $z = 3$ .  $V_{\text{H}}$  is evaluated by solving the Poisson equation,

$$\Delta V_{\text{H}}[n_e(\mathbf{r}, t)] = -4\pi e n_e(\mathbf{r}, t). \quad (10)$$

Here, let us introduce a real-space simulation box  $\Omega$ , on which the periodic boundary condition is imposed, and translation vectors  $\mathbf{G}$ .  $\Omega$  is defined as,

$$\Omega = \left\{ \mathbf{r} = \sum_{j=x,y,z} a_j \mathbf{e}_j \mid 0 \leq a_j < 1 \right\}, \quad (11)$$

where  $\{\mathbf{e}_j\}$  are the lattice vectors along the  $j$ -axis ( $j = x, y, z$ ), whose lengths are denoted by  $L_j = |\mathbf{e}_j|$ . Integrals with respect to  $\mathbf{r}$  are taken over  $\Omega$  in what follows. The translation vectors are given by,

$$\mathbf{G} = \sum_{j=x,y,z} M_j \mathbf{e}_j \quad (M_j = 0, \pm 1, \pm 2, \dots). \quad (12)$$

Taking the periodic boundary condition into account, the Coulomb terms  $V_{\text{ps}}$  and  $V_{\text{H}}$  are represented as a Fourier series expansion. The pseudo potential term is rewritten as,

$$\sum_i^\infty V_{\text{ps}}(\mathbf{r} - \mathbf{r}_i) = \sum_{\mathbf{G}, i=1}^{N_{\text{ion}}} V_{\text{ps}}(\mathbf{r} - \mathbf{r}_i - \mathbf{G}), \quad (13)$$

where  $N_{\text{ion}}$  denotes the number of ions in  $\Omega$  and,

$$\begin{aligned} & \sum_{\mathbf{G}} V_{\text{ps}}(\mathbf{r} - \mathbf{r}_i - \mathbf{G}) \\ &= \mathcal{F}^{-1} \left[ \sum_i e^{-\mathbf{Q} \cdot \mathbf{r}_i} \left\{ V_{\text{ps}}(Q) + \frac{4\pi}{Q} z \right\} \right]. \end{aligned} \quad (14)$$

with  $\mathbf{Q}$  being the coordinates in the Fourier domain ( $Q = |\mathbf{Q}|$ ),  $\mathcal{F}[\cdot]$  the Fourier series expansion within  $\Omega$ , and,

$$\begin{aligned} V_{\text{ps}}(Q) = 4\pi z e R^2 & \left[ -\frac{1}{(QR)^2} + \frac{1}{(QR)^2 + \alpha^2} \right. \\ & \left. + \frac{2\alpha\beta}{\{(QR)^2 + \alpha^2\}^2} + \frac{2A}{\{(QR)^2 + 1\}^2} \right], \end{aligned} \quad (15)$$

One obtains the solution of the Poisson equation (Eq. (10)) for the electron density  $n_e$  given within  $\Omega$  as,

$$V_{\text{H}}[n_e(\mathbf{r}, t)] = \mathcal{F}^{-1} \left[ \mathcal{F}[n_e(\mathbf{r}, t)] \frac{4\pi e}{Q^2} \right]. \quad (16)$$

For the exchange-correlation potential  $V_{\text{xc}}$ , one employs the LDA by Perdew and Zunger [58]. The laser-electron interaction is described in the length gauge,

$$V_{\text{ext}}(\mathbf{r}, t) = -e\mathbf{E}(t) \cdot \mathbf{r}, \quad (17)$$

within the dipole approximation, where  $\mathbf{E}$  denotes the laser electric field vector. In this case,  $\mathbf{p}$  becomes the kinetic momentum, and, thus, the electronic current density  $\mathbf{J}(t)$  averaged over  $\Omega$  is given by,

$$\mathbf{J}(t) = \frac{1}{|\Omega|} \iint_{\Omega} \left( -e \frac{\mathbf{p}}{m} \right) f(\mathbf{r}, \mathbf{p}, t) d\mathbf{r} d\mathbf{p}. \quad (18)$$

## B. Numerical implementations

### 1. Pseudo-particle method

The direct propagation of the distribution function would require the treatment of six-dimensional time-dependent function on grids [59]. To avoid such a massive computation, one introduces the pseudo-particle method [46–48, 60], where the distribution function  $f(\mathbf{r}, \mathbf{p}, t)$  is expressed by a set of pseudo-particles with mass  $m$  as,

$$f(\mathbf{r}, \mathbf{p}, t) = \frac{1}{N_s} \sum_{i=1}^{N_{\text{pp}}} g_r(\mathbf{r} - \mathbf{r}_i(t)) g_p(\mathbf{p} - \mathbf{p}_i(t)). \quad (19)$$

Here  $\mathbf{r}_i, \mathbf{p}_i$  are the position and canonical momentum of each pseudo particle labeled by  $i$ . The total number of pseudo particles  $N_{\text{pp}}$  is given by  $N_{\text{pp}} = N_s N_e$ , where  $N_s$  and  $N_e$  are the number of pseudo particles per electron and the total number of the electrons contained in  $\Omega$ , respectively. Statistical error is reduced by increasing  $N_s$ .  $N_s$  is set to 10000 in this study.  $g_r(\mathbf{r})$  and  $g_p(\mathbf{p})$  denote smoothing kernel functions for the position and momentum, respectively, of Gaussian forms,

$$g_r(\mathbf{r}) = \sum_{\{\mathbf{G}\}} \frac{1}{\pi^{3/2} d_r^3} \exp(-|\mathbf{r} + \mathbf{G}|^2 / d_r^2), \quad (20)$$

$$g_p(\mathbf{p}) = \frac{1}{\pi^{3/2} d_p^3} \exp(-|\mathbf{p}|^2 / d_p^2), \quad (21)$$

where  $d_r$  and  $d_p$  are smoothing widths. Only the nearest neighbor cells are included in summation over  $\mathbf{G}$  in Eq. (20). The kernel functions are normalized as,

$$\int_{\Omega} g_r(\mathbf{r}) d\mathbf{r} = 1, \quad (22)$$

$$\int g_p(\mathbf{p}) d\mathbf{p} = 1, \quad (23)$$

so that,

$$\iint_{\Omega} f(\mathbf{r}, \mathbf{p}, t) d\mathbf{r} d\mathbf{p} = N_e. \quad (24)$$

The scattering cross-section of the electron and the effective potential is adjusted through  $d_r$ ; the smaller  $d_r$ , the larger the cross-section. Here we use  $d_r = 0.575$  a.u. so that the time-dependent energy absorption reproduces the TDLDA results. In the present collision-less case,  $d_p$  is not used explicitly.

The field quantities such as  $V_{\text{eff}}$  and  $n_e$  are evaluated on three-dimensional grids discretized into  $N_j$  ( $j = x, y, z$ ) intervals on the  $j$  axis with a spatial step  $\Delta j = L_j / N_j$ . In our calculation we set  $\Delta x = \Delta y = \Delta z = 0.5$  a.u. Here,  $d_r / \Delta x \simeq 1.15$  is a good parameterization leading to stable simulation [47]. It should be noticed that  $d_r$  is the only adjustable parameter in our formalism. The electron density on a grid point  $\mathbf{r}$  is calculated as,

$$n_e(\mathbf{r}, t) = \int d\mathbf{p} f(\mathbf{r}, \mathbf{p}, t) = \frac{1}{N_s} \sum_{i=1}^{N_{\text{pp}}} g_r(\mathbf{r}_i(t) - \mathbf{r}). \quad (25)$$

The current density  $\mathbf{J}(t)$  [Eq. (18)] is evaluated as,

$$\mathbf{J}(t) = -\frac{1}{|\Omega|} \frac{e}{N_s} \sum_{i=1}^{N_{\text{pp}}} \frac{\mathbf{p}_i(t)}{m}. \quad (26)$$

The Hamiltonian in pseudo-particle representation is written as,

$$H_{\text{pp}} = \frac{1}{N_s} \sum_i^{N_{\text{pp}}} \left[ \frac{\mathbf{p}_i^2(t)}{2m} + \int_{\Omega} V_{\text{eff}}(\mathbf{r}, t) g_r(\mathbf{r}_i - \mathbf{r}) d\mathbf{r} \right]. \quad (27)$$

The motion of each pseudo particle is governed by the Newton equations under the effective potential  $V_{\text{eff}}$  with the periodic boundary condition as,

$$\dot{\mathbf{r}}_i = \frac{\mathbf{p}_i}{m}, \quad \dot{\mathbf{p}}_i = - \int_{\Omega} V_{\text{eff}}(\mathbf{r}) \nabla_{\mathbf{r}_i} g_r(\mathbf{r}_i - \mathbf{r}) d\mathbf{r}. \quad (28)$$

As long as pseudo-particle canonical variables  $\mathbf{r}_i, \mathbf{p}_i$  obey the Newton equation (Eq. (28)), one-body distribution (Eq. (19)) satisfies the Vlasov equation (Eq. (6)). The force term is given as the gradient of the  $N_{\text{pp}}$ -body Hamiltonian  $H_{\text{pp}}$ . One numerically integrates it as,

$$\begin{aligned} \int V_{\text{eff}}(\mathbf{r}) \nabla_{\mathbf{r}} g_r(\mathbf{r}_i - \mathbf{r}) d\mathbf{r} \\ \simeq \sum_{\mathbf{r} \in \Omega} V_{\text{eff}}(\mathbf{r}) \nabla_{\mathbf{r}_i} g_r(\mathbf{r}_i - \mathbf{r}) \Delta x \Delta y \Delta z, \end{aligned} \quad (29)$$

using the analytical form of  $\nabla_{\mathbf{r}_i} g_r(\mathbf{r}_i - \mathbf{r})$ ,

$$\begin{aligned} \nabla_{\mathbf{r}_i} g_r(\mathbf{r}_i - \mathbf{r}) \\ = \sum_{\{\mathbf{G}\}} \frac{-2(\mathbf{r}_i - \mathbf{r} + \mathbf{G})}{\pi^{3/2} d_r^5} \exp(-|\mathbf{r}_i - \mathbf{r} + \mathbf{G}|^2 / d_r^2). \end{aligned} \quad (30)$$

The integration of Eq. (28) is performed by the Verlet method [61] with time step  $\Delta t = 0.02$  a.u. Particles exiting  $\Omega$  are to re-enter  $\Omega$  from the other side.

## 2. Ground state

The initial state is the stationary solution of the Vlasov equation described by the Thomas-Fermi model. The total energy functional,

$$\begin{aligned} E_{\text{all}}[n_e(\mathbf{r})] = \int_{\Omega} \left[ \frac{3}{10} \frac{\hbar^2 (3\pi^2)^{2/3}}{m} n_e^{5/3}(\mathbf{r}) + \frac{1}{2} V_{\text{H}}(\mathbf{r}) n_e(\mathbf{r}) \right. \\ \left. + \sum_{\mathbf{G}, i=1}^{N_{\text{ion}}} V_{\text{ps}}(\mathbf{r} - \mathbf{r}_i - \mathbf{G}) n_e(\mathbf{r}) + E_{\text{xc}}[n_e(\mathbf{r})] \right] d\mathbf{r}, \end{aligned} \quad (31)$$

is variationally minimized with respect to  $n_e(\mathbf{r})$  under the constraint that the box  $\Omega$  contains  $N_e$  electrons. This leads to the following coupled equations,

$$\frac{\hbar^2}{2m} [3\pi^2 n_e(\mathbf{r})]^{2/3} + V_{\text{eff}}(\mathbf{r}) = \mu, \quad (32)$$

$$V_{\text{eff}}(\mathbf{r}) = V_{\text{Coulomb}}[n_e(\mathbf{r})] + V_{\text{xc}}[n_e(\mathbf{r})], \quad (33)$$

where  $\mu$  denotes the chemical potential, playing the role of a Lagrange multiplier. These equations are to be solved for  $n_e(\mathbf{r})$  self-consistently.

An adopted algorithm to solve the coupled equations Eq. (32) and Eq. (33) is shown in Fig. 1.

First, the chemical potential  $\mu$  and the electron density  $n_e^{\text{in}}$  in the real space are guessed so that the total

```

1: procedure GROUND STATE PREPARATION
2:   (–Initialization–)
3:   initial guess of  $\mu$  and  $n_e^{\text{in}}$ 
4:
5:   (–Self-consistent determination of  $\mu$  and  $n_e$ –)
6:   while  $\Delta n > \epsilon$  ( $\epsilon = 10^{-7}$ ) do
7:     set pseudo-particle position  $\{\mathbf{r}_i\}$ 
8:      $\{\mathbf{r}_i\} \mapsto n_{\text{ps}}(\mathbf{r})$  using Eq. (25)
9:      $n_{\text{ps}} \mapsto V_{\text{eff}}[n_{\text{ps}}](\mathbf{r})$  using Eq. (33)
10:     $V_{\text{eff}}[n_{\text{ps}}](\mathbf{r}) \mapsto n_e$ 
11:    find appropriate  $\mu$ 
12:     $\Delta n = \int_{\Omega} d\mathbf{r} |n_e^{\text{in}}(\mathbf{r}) - n_e(\mathbf{r})|$ 
13:     $n_e^{\text{in}} = n_e$ 
14:  end while
15:
16:  (–Set Pseudo-particle Momenta–)
17:  for  $i = 1, N_{\text{pp}}$  do
18:    while  $p > p_f$  do
19:      random number  $p_x$  ( $0 \leq |p_x| \leq p_f$ )
20:      random number  $p_y$  ( $0 \leq |p_y| \leq p_f$ )
21:      random number  $p_z$  ( $0 \leq |p_z| \leq p_f$ )
22:       $p = \sqrt{p_x^2 + p_y^2 + p_z^2}$ 
23:    end while
24:     $\mathbf{p}_i = (p_x, p_y, p_z)$ 
25:  end for
26: end procedure

```

FIG. 1. Algorithm for the ground state preparation

number of electrons within  $\Omega$  is  $N_e$  (line 3). Then, one distributes pseudo particles according to the guessed  $n_e^{\text{in}}$  using random numbers (line 7, also see below). The electron density  $n_{\text{ps}}$  realized by the pseudo-particle distribution is calculated through Eq. (25) (line 8). The effective potential  $V_{\text{eff}}(\mathbf{r})$  is obtained by substituting  $n_{\text{ps}}$  into the right-hand side of Eq. (33) (line 9). Then, we update the electron density  $n_e(\mathbf{r})$  by substituting thus obtained  $V_{\text{eff}}(\mathbf{r})$  to the Eq. (32) and solving it with respect to  $n_e$  (line 10), simultaneously updating  $\mu$  by a bisection method to satisfy the condition that the total number of electrons is  $N_e$  (line 11). The updated  $n_e$  is used as  $n_e^{\text{in}}$  in the next iteration of the loop (line 13). One repeats the above operations till convergence,  $\int_{\Omega} d\mathbf{r} |n_e^{\text{in}} - n_e| < \epsilon$ , where we set  $\epsilon = 10^{-7}$  here for crystalline Al (line 12). After convergence, one distributes the momenta of the pseudo particles uniformly within the local Fermi radius  $p_f$  by acceptance-rejection sampling of uniform pseudo-random numbers (lines 17-25).

The algorithm to distribute the pseudo particles (line 7 in Fig. 1) is shown in Fig. 2.

We introduce sub-grid points (line 3) by dividing each voxel of the computational grid into  $N_{\text{inp}}^j$  regions along the  $j$ -axis ( $j = x, y, z$ ). The electron density  $n_e^{\text{inp}}$  on each sub-grid point is evaluated, based on the trilinear interpolation from those of the surrounding eight computational grid points, from which one calculates the number of pseudo particles  $N_{\text{pp}}^{\text{local}}$  around the sub-grid point (lines 4-5). Then, the  $N_{\text{pp}}^{\text{local}}$  pseudo particles are uniformly distributed around the sub-grid point using random num-

```

1: procedure HOW TO SET PSEUDO PARTICLE POSITION
2:   (-# of Pseudo Particles around  $\mathbf{r}_s$ -)
3:   a sub-grid point  $\mathbf{r}_s = (x_s, y_s, z_s)$ 
4:   calculate  $n_e^{\text{inp}}(\mathbf{r}_s)$  by interpolation
5:   the number of pseudo particles  $n_e^{\text{inp}} \mapsto N_{\text{pp}}^{\text{local}}$ 
6:
7:   (-Distribute Pseudo Particles around  $\mathbf{r}_s$ -)
8:   for  $l = 1, N_{\text{pp}}^{\text{local}}$  do
9:     random number  $R_x$  ( $-0.5 \leq R_x \leq 0.5$ )
10:    random number  $R_y$  ( $-0.5 \leq R_y \leq 0.5$ )
11:    random number  $R_z$  ( $-0.5 \leq R_z \leq 0.5$ )
12:     $x_l = x_s + R_x L_x / N_{\text{inp}}^x$ 
13:     $y_l = y_s + R_y L_y / N_{\text{inp}}^y$ 
14:     $z_l = z_s + R_z L_z / N_{\text{inp}}^z$ 
15:     $l$ -th pseudo particle position is
16:     $\mathbf{r}_l = (x_l, y_l, z_l)$ 
17:   end for
18: end procedure

```

FIG. 2. Algorithm for pseudo particle distribution

bers (lines 8-17).

### C. Linear response

We evaluate the linear optical response via impulse response by doing dynamical simulations with the initial pseudo-particle momenta  $\mathbf{p}_i$  shifted from the ground-state values  $\mathbf{p}_i^{\text{GS}}$  by a small amount  $\Delta\mathbf{p}$ ,

$$\mathbf{p}_i = \mathbf{p}_i^{\text{GS}} + \Delta\mathbf{p}, \quad (34)$$

where  $\Delta\mathbf{p} = (0, 0, 0.1 \text{ a.u.})$  in this study. This is equivalent to the application of an impulse electric field,

$$\mathbf{E}(t) = -\frac{1}{e}\Delta\mathbf{p}\delta(t), \quad (35)$$

where  $\delta(t)$  is the delta function. Noting that this field has a constant power spectrum across all frequencies, one can readily obtain the optical conductivity as,

$$\sigma_{mn}(\omega) = -\frac{e\hat{J}_m(\omega)}{\Delta p_n} \quad (m, n = x, y, z), \quad (36)$$

where  $\Delta p_m$  and  $\hat{J}_m$  ( $m, n = x, y, z$ ) denote the  $m$  component of the momentum shift and the temporal Fourier transform of the current density, respectively. The fast Fourier transformation algorithm [62] is used for the evaluation of  $\hat{J}_m(\omega)$ . Assuming isotropic media, the dielectric function  $\varepsilon_{mm}(\omega)$ , the complex refractive index  $n(\omega)$ , and the reflectivity  $R(\omega)$  are given by,

$$\varepsilon_{mm}(\omega) = 1 + 4\pi i \frac{\sigma_{mm}(\omega)}{\omega}, \quad (37)$$

$$n(\omega) = \sqrt{\varepsilon_{mm}(\omega)}, \quad (38)$$

$$R(\omega) = \left| \frac{\sqrt{\varepsilon_{mm}(\omega)} - 1}{\sqrt{\varepsilon_{mm}(\omega)} + 1} \right|^2, \quad (39)$$

respectively, especially,  $\varepsilon_{xx}(\omega) = \varepsilon_{yy}(\omega) = \varepsilon_{zz}(\omega)$ .

## III. RESULTS

In this section, we compare the results of the Vlasov-LDA simulations for extended systems described in the previous section with the experimental values and the TDDFT results obtained by the open source code SALMON [37, 63, 64]. We take aluminum as a target material. For Vlasov-LDA, simulation parameters are  $N_s = 10000$ ,  $N_e = 12$ , and time step  $\Delta t = 0.025 \text{ a.u.}$ . For TDDFT, we employ a norm-conserving pseudopotential [65] and the LDA functional [58], with the number of k-points  $48^3$ , number of real-space grids  $14^3$ , and  $dt = 0.15 \text{ a.u.}$  We assume an external electric field linearly polarized along the  $\Gamma - X$  direction of the following temporal profile:

$$E(t) = E_0 \sin \left[ \omega \left( t - \frac{T}{2} \right) \right] \sin^2 \left( \frac{t}{T} \pi \right) \quad (0 \leq t \leq T), \quad (40)$$

where  $E_0$  denotes the field amplitude,  $\hbar\omega$  the photon energy, and  $T$  the (foot-to-foot) full pulse duration. The corresponding full width at half maximum duration of the laser intensity profile is about  $0.36T$ .

### A. Linear response

Let us first discuss the complex optical conductivity, refractive index, extinction coefficient, and reflectivity as a function of photon energy. Despite the simplicity of the Vlasov-LDA approach, its results excellently agree with the TDDFT results and experimental values (Fig. 3), especially above 2 eV photon energy. The peak and dip around 1.5 eV in the TDDFT results are due to interband absorption, which is not reproduced by the present Vlasov approach, since the latter takes only the single free-electron dispersion into account. Focusing on reflectivity behavior around the plasma frequency, one finds some differences between the two approaches. This difference would be contributions by the above-mentioned interband resonance and non-unity effective mass in TDDFT. We have confirmed it through the decomposition of the response obtained by TDDFT into Drude and Lorentz model components. With the resonance energy set to 1.85 eV, the biggest oscillator around 1.5 eV [67], The estimated effective mass  $m_{\text{eff}}$  is  $1.09m$ , and the damping constant is  $0.51 \text{ eV}^{-1}$ , consistent with the values reported previously ( $1.16m$  [68] and  $0.80 \text{ eV}^{-1}$  [67], respectively). The loss functions,  $\text{Im}\epsilon(\omega)^{-1}$ , are shown in Fig. 4. The TDDFT result is excellently reproduced by the combined Drude and Lorentz contributions with  $m_{\text{eff}} = 1.09m$ . Although Vlasov-LDA overestimates the plasma frequency compared to TDDFT, it agrees with the Drude model with  $m_{\text{eff}} = m$ .



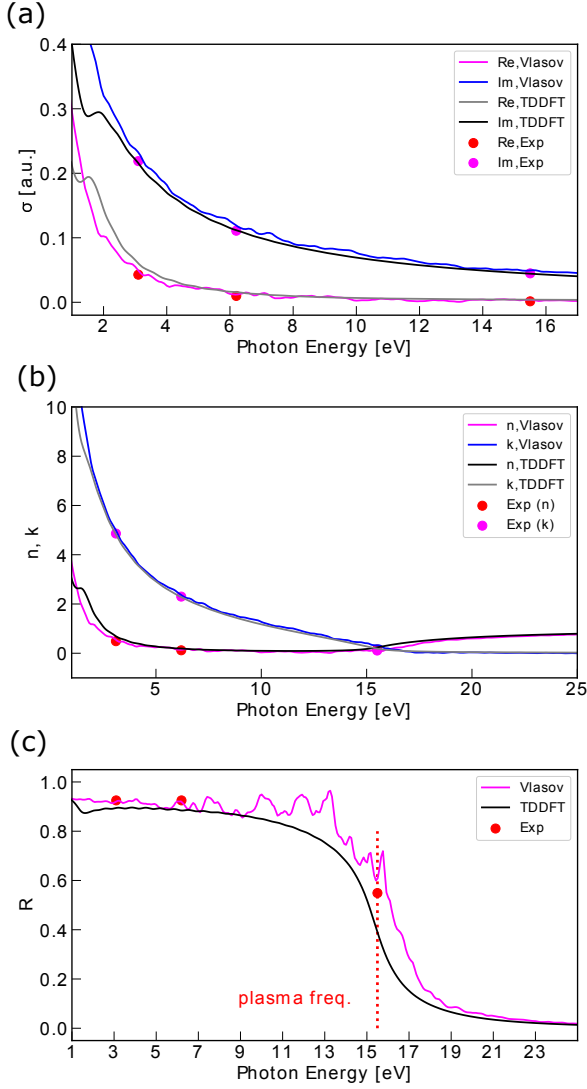


FIG. 3. (a) Optical conductivity  $\sigma(\omega)$ , (b) refractive index  $n$  and extinction coefficient  $k$ , (c) reflectivity  $R(\omega)$ , calculated with the Vlasov-LDA method and TDDFT as well as reported in experimental reference [66]. The experimental values are plotted at 3.1 eV (400 nm), 6.2 eV (200 nm), and 15.5 eV (80 nm).

### B. Energy absorption

Let us next investigate the energy absorption from the laser pulse. We evaluate the energy absorption by the electrons as their energy increment by the pulse irradiation. The energy is calculated as  $\Delta E = H_{pp}(t = \infty) - H_{pp}(t = 0)$  in the Vlasov-LDA simulation and as  $\langle h_{KS}(t = \infty) \rangle - \langle h_{KS}(t = 0) \rangle$  in the TDDFT simulation. We show the fluence dependence for the fixed intensity ( $10^{12}$  W/cm<sup>2</sup>) at 80 nm wavelength in Fig. 5 and that for the fixed pulse width of 3.8 fs at 200 and 400 nm wavelengths in Fig. 7.

We see in Fig. 5 that both Vlasov-LDA and TDDFT results are linear in fluence and agree well with each other

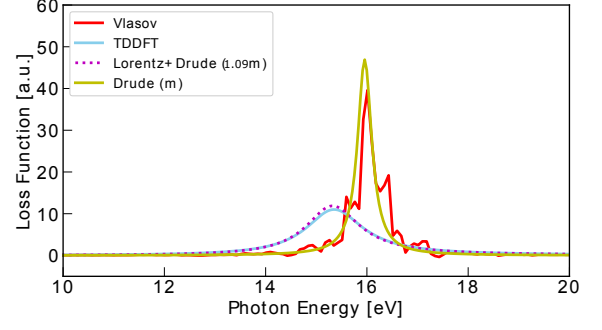


FIG. 4. Loss functions by TDDFT, Vlasov-LDA, combined Drude and Lorentz models ( $m_{\text{eff}} = 1.09m$ ), and Drude model ( $m_{\text{eff}} = m$ ). The peak of the loss function gives plasma frequency.

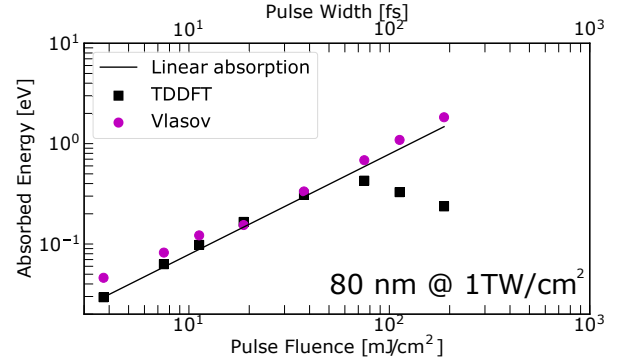


FIG. 5. Calculated absorbed energy vs. pulse fluence or pulse width for a fixed intensity (1 TW/cm<sup>2</sup>). Pink circles: Vlasov-LDA, black squares: TDDFT, solid line: linear dependence passing through the square (TDDFT) for the 3.8 fs pulse.

in the lower fluence region ( $\lesssim 50$  mJ/cm<sup>2</sup>). On the other hand, the Vlasov-LDA does not reproduce the TDDFT results for the higher fluence, where the latter deviate from the linear behavior and even decrease with increasing fluence. This difference is due to Rabi-like oscillation [69], as confirmed in Fig. 6, which shows the temporal evolution of absorbed energy for several pulse widths. The maximum electron energy gain during the pulse, which are indicated by horizontal dashed lines, does not depend much on the pulse width, suggesting Rabi-like coherent oscillation. Thus, there is an optimum pulse width for a fixed intensity in terms of energy absorption.

Figure 7 indicates that the energy absorption calculated by the Vlasov-LDA approach exhibit a linear dependence on fluence or pulse intensity in the whole range. We can see a nonlinear behavior, on the other hand, in the TDDFT results in the higher fluence range ( $\gtrsim 40$  mJ/cm<sup>2</sup> for 200 nm and  $\gtrsim 2$  mJ/cm<sup>2</sup> for 400 nm). This would be interpreted as saturable absorption as is widely observed in various materials [70]. We could not obtain the Vlasov-LDA results for the low fluence region ( $\lesssim 2$  mJ/cm<sup>2</sup>) because of statistical error. This could be

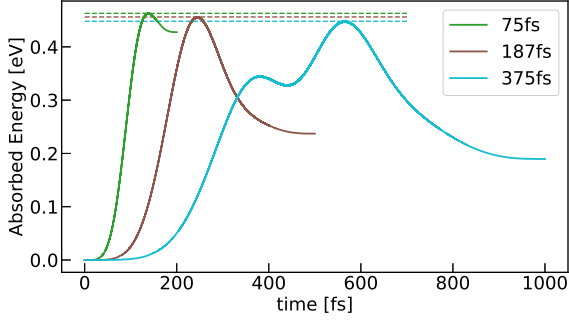


FIG. 6. Solid lines: temporal evolution of the absorbed energy for three different pulse widths 75, 187, and 375 fs. Dashed lines: maximum values for each pulse width.

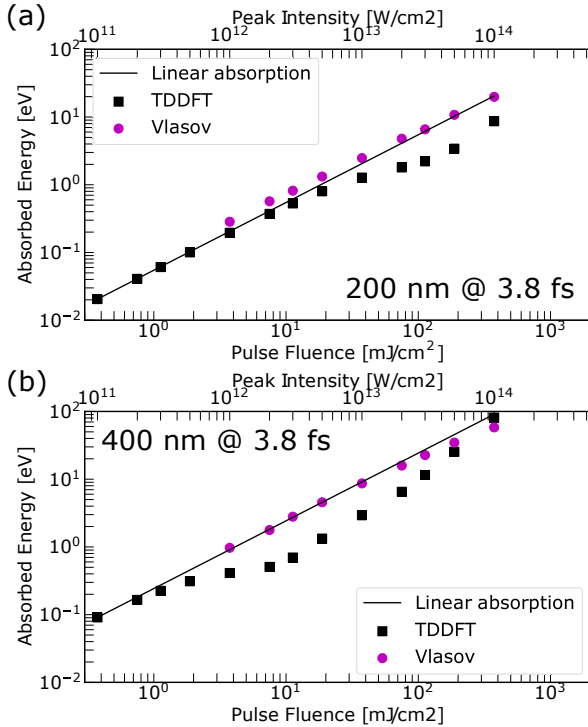


FIG. 7. Absorbed energy vs. pulse fluence or peak intensity for a fixed pulse width of 3.8 fs for the case of (a) 200 nm and (b) 400 nm wavelength. Pink circles: Vlasov-LDA, black squares: TDDFT, solid line: linear dependence passing through the square (TDDFT) for  $10^{11} \text{ W/cm}^2$  intensity.

improved by increasing the total number of pseudo particles, in principle. Nevertheless, the Vlasov-LDA results, if extrapolated to the low fluence region, appear to agree well with the TDDFT results.

Figure 8 shows the temporal evolution of the current density and absorbed energy for  $10^{12} \text{ W/cm}^2$  peak intensity, 200 nm wavelength, and 3.8 fs pulse width. Again, overall, the Vlasov results excellently reproduce the TDDFT results. In Fig. 8 (b), although energy fluctuation due to the pseudo-particle statistical error is seen

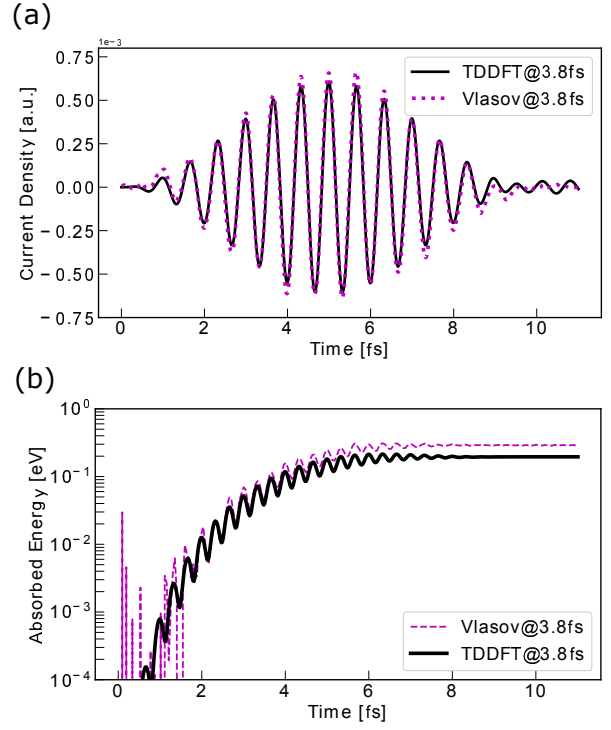


FIG. 8. (a) Time-dependent current density  $J(t)$  and (b) electron energy absorption  $\Delta E(t)$ . Pink dashed lines: Vlasov-LDA, black solid lines: TDDFT.

at  $< 2$  fs, it becomes negligible at the end of the pulse.

Our code is partially parallelized using OpenMP and MPI. One of the most time-consuming parts is the Fourier transformation, which is computed by naive approach. Nevertheless, the computational time of the present Vlasov-LDA code is typically only 1/20 of that of TDDFT using the SALMON code. With more sophistication and parallelization, the efficiency of the Vlasov-LDA method will be further improved, which will be advantageous for applications such as parameter optimization in laser material processing.

#### IV. CONCLUSIONS

We have extended the Vlasov-LDA semi-classical approach and implemented it with the pseudo-particle method to periodic systems in order to compute the electron dynamics in solids, especially in metals, under ultra-short intense laser pulses. The Vlasov equation can be regarded as the leading order of a semiclassical  $\hbar$  expansion of the time-dependent Kohn-Sham equations. The electronic distribution function is expressed by pseudo-particles, incorporating the periodic boundary condition. They play the role of Lagrangian markers embedded randomly in the electron gas. The initial distribution is calculated from the Thomas-Fermi model.

We have applied this approach to crystalline aluminum. Although the method has only one adjustable

parameter  $d_r$ , the calculated optical conductivity, refractive index, extinction coefficient, and reflectivity as well as energy absorption are overall in excellent agreement with the TDDFT and experimental results over a wide range of photon energy and fluence, demonstrating the capability of the present approach to accurately describe the dynamics of metallic conduction-band electrons. On the other hand, the Vlasov results deviate from the TDDFT ones around 1.5 eV photon energy, where interband transitions are involved, and at the high-fluence region, where a Rabi-like oscillation takes place.

The next step will be to incorporate electron-electron collisions, the description of which is limited in TDDFT. Vlasov-LDA is expected to provide valuable insights into complex laser-material processing if we further couple it with molecular dynamics, electromagnetic field analysis, and other continuum models.

### ACKNOWLEDGEMENTS

We wish to express our gratitude to Kazuhiro Yabana for private discussions. This research was supported

by MEXT Quantum Leap Flagship Program (MEXT Q-LEAP) Grant Number JPMXS0118067246. This research was also partially supported by JSPS KAKENHI Grant Number 20H05670, JST COI Grant Number JPMJCE1313, and JST CREST under Grant Number JPMJCR16N5. M.T. gratefully acknowledges support from the Graduate School of Engineering, The University of Tokyo, Graduate Student Special Incentives Program. M.T. also gratefully thanks support through crowd funding platform *academist* by Misako Abe, Daigo Oue, Miho Otsuka, Yusaku Karibe, Ayano Sakai, Yushi Sakai, Shunsuke A. Sato, Ryosuke Shibato, Hitomi Suto, Tomoharu Sunouchi, Hideo Takahashi, and Yusuke Tokunaga. The numerical calculations are partially performed on supercomputers Oakbridge-CX, sekirei, ohtaka (the University of Tokyo), and SGI ICE X at Japan Atomic Energy Agency(JAEA). This research is partially supported by Initiative on Promotion of Supercomputing for Young or Women Researchers, Information Technology Center, The University of Tokyo.

- 
- [1] S. Ghimire, A. D. DiChiara, E. Sistrunk, P. Agostini, L. F. DiMauro, and D. A. Reis, Observation of high-order harmonic generation in a bulk crystal, *Nature physics* **7**, 138 (2011).
  - [2] G. Vampa, T. Hammond, N. Thiré, B. Schmidt, F. Légaré, C. McDonald, T. Brabec, and P. Corkum, Linking high harmonics from gases and solids, *Nature* **522**, 462 (2015).
  - [3] Y. S. You, D. A. Reis, and S. Ghimire, Anisotropic high-harmonic generation in bulk crystals, *Nature physics* **13**, 345 (2017).
  - [4] G. Ndabashimiye, S. Ghimire, M. Wu, D. A. Browne, K. J. Schafer, M. B. Gaarde, and D. A. Reis, Solid-state harmonics beyond the atomic limit, *Nature* **534**, 520 (2016).
  - [5] Y. Morimoto, Y. Shinohara, M. Tani, B.-H. Chen, K. L. Ishikawa, and P. Baum, Asymmetric single-cycle control of valence electron motion in polar chemical bonds, *Optica* **8**, 382 (2021).
  - [6] C. Schaefer, H. M. Urbassek, and L. V. Zhigilei, Metal ablation by picosecond laser pulses: A hybrid simulation, *Physical review B* **66**, 115404 (2002).
  - [7] C. Kerse, H. Kalaycıoğlu, P. Elahi, B. Çetin, D. K. Kesim, Ö. Akçaalan, S. Yavaş, M. D. Aşık, B. Öktem, H. Hoogland, R. Holzwarth, and F. Ö. Ilday, Ablation-cooled material removal with ultrafast bursts of pulses, *Nature* **537**, 84 (2016).
  - [8] J.-P. Colombier, P. Combis, F. Bonneau, R. Le Harzic, and E. Audouard, Hydrodynamic simulations of metal ablation by femtosecond laser irradiation, *Physical review B* **71**, 165406 (2005).
  - [9] V. Schmidt, W. Husinsky, and G. Betz, Dynamics of laser desorption and ablation of metals at the threshold on the femtosecond time scale, *Physical review letters* **85**, 3516 (2000).
  - [10] K.-H. Leitz, B. Redlingshöfer, Y. Reg, A. Otto, and M. Schmidt, Metal ablation with short and ultrashort laser pulses, *Physics Procedia* **12**, 230 (2011).
  - [11] B. N. Chichkov, C. Momma, S. Nolte, F. Von Alvensleben, and A. Tünnermann, Femtosecond, picosecond and nanosecond laser ablation of solids, *Applied physics A* **63**, 109 (1996).
  - [12] X. Liu, D. Du, and G. Mourou, Laser ablation and micromachining with ultrashort laser pulses, *IEEE journal of quantum electronics* **33**, 1706 (1997).
  - [13] S. Amoruso, G. Ausanio, R. Bruzzese, M. Vitiello, and X. Wang, Femtosecond laser pulse irradiation of solid targets as a general route to nanoparticle formation in a vacuum, *Physical Review B* **71**, 033406 (2005).
  - [14] E. G. Gamaly, The physics of ultra-short laser interaction with solids at non-relativistic intensities, *Physics Reports* **508**, 91 (2011).
  - [15] N. Medvedev, H. O. Jeschke, and B. Ziaja, Nonthermal phase transitions in semiconductors induced by a femtosecond extreme ultraviolet laser pulse, *New Journal of Physics* **15**, 015016 (2013).
  - [16] R. R. Gattass and E. Mazur, Femtosecond laser micromachining in transparent materials, *Nature photonics* **2**, 219 (2008).
  - [17] I. Mirza, N. M. Bulgakova, J. Tomášťík, V. Michálek, O. Haderka, L. Fekete, and T. Mocek, Ultrashort pulse laser ablation of dielectrics: Thresholds, mechanisms, role of breakdown, *Scientific reports* **6**, 1 (2016).
  - [18] E. Silaeva, A. Vella, N. Sevelin-Radiguet, G. Martel, B. Deconihout, and T. Itina, Ultrafast laser-triggered field ion emission from semiconductor tips, *New Journal of Physics* **14**, 113026 (2012).



- [19] B. Rethfeld, D. S. Ivanov, M. E. Garcia, and S. I. Anisimov, Modelling ultrafast laser ablation, *Journal of Physics D: Applied Physics* **50**, 193001 (2017).
- [20] B. Rethfeld, Unified model for the free-electron avalanche in laser-irradiated dielectrics, *Physical review letters* **92**, 187401 (2004).
- [21] A. Rudenko, J.-P. Colombier, and T. E. Itina, From random inhomogeneities to periodic nanostructures induced in bulk silica by ultrashort laser, *Physical Review B* **93**, 075427 (2016).
- [22] B. Chimier, O. Utéza, N. Sanner, M. Sentis, T. Itina, P. Lassonde, F. Légaré, F. Vidal, and J. Kieffer, Damage and ablation thresholds of fused-silica in femtosecond regime, *Physical Review B* **84**, 094104 (2011).
- [23] P. Lorazo, L. J. Lewis, and M. Meunier, Thermodynamic pathways to melting, ablation, and solidification in absorbing solids under pulsed laser irradiation, *Physical Review B* **73**, 134108 (2006).
- [24] J. Thorstensen and S. Erik Foss, Temperature dependent ablation threshold in silicon using ultrashort laser pulses, *Journal of Applied Physics* **112**, 103514 (2012).
- [25] T. Kondo, S. Matsuo, S. Juodkazis, V. Mizeikis, and H. Misawa, Multiphoton fabrication of periodic structures by multibeam interference of femtosecond pulses, *Applied Physics Letters* **82**, 2758 (2003).
- [26] A. K. Upadhyay, N. A. Inogamov, B. Rethfeld, and H. M. Urbassek, Ablation by ultrashort laser pulses: Atomistic and thermodynamic analysis of the processes at the ablation threshold, *Physical Review B* **78**, 045437 (2008).
- [27] D. Ivanov, A. Kuznetsov, V. Lipp, B. Rethfeld, B. Chichkov, M. Garcia, and W. Schulz, Short laser pulse nanostructuring of metals: direct comparison of molecular dynamics modeling and experiment, *Applied Physics A* **111**, 675 (2013).
- [28] D. Ivanov, V. Lipp, A. Blumenstein, F. Kleinwort, V. Veiko, E. Yakovlev, V. Roddatis, M. Garcia, B. Rethfeld, J. Ihlemann, and P. Simon, Experimental and theoretical investigation of periodic nanostructuring of au with ultrashort uv laser pulses near the damage threshold, *Physical Review Applied* **4**, 064006 (2015).
- [29] T. E. Itina, K. Gouriet, L. V. Zhigilei, S. Noël, J. Hermann, and M. Sentis, Mechanisms of small clusters production by short and ultra-short laser ablation, *Applied Surface Science* **253**, 7656 (2007).
- [30] B. J. Garrison, T. E. Itina, and L. V. Zhigilei, Limit of overheating and the threshold behavior in laser ablation, *Physical Review E* **68**, 041501 (2003).
- [31] S. Sakabe, M. Hashida, S. Tokita, S. Namba, and K. Okamuro, Mechanism for self-formation of periodic grating structures on a metal surface by a femtosecond laser pulse, *Physical Review B* **79**, 033409 (2009).
- [32] M. Ishino, N. A. Inogamov, S. Tamotsu, V. V. Zhakhovsky, N. Hasegawa, I. Y. Skobelev, A. Y. Faenov, T. A. Pikuz, K. Mikami, T. Kawachi, and M. Nishikino, Study of damage structure formation on aluminum film targets by picosecond soft x-ray laser ablation around threshold region, *Applied Physics A* **124**, 1 (2018).
- [33] J. Anthes, M. Gusinow, and M. K. Matzen, Experimental observation and numerical simulations of laser-driven ablation, *Physical Review Letters* **41**, 1300 (1978).
- [34] B. J. Simonds, J. Sowards, J. Hadler, E. Pfeif, B. Wilthan, J. Tanner, C. Harris, P. Williams, and J. Lehman, Time-resolved absorptance and melt pool dynamics during intense laser irradiation of a metal, *Physical review applied* **10**, 044061 (2018).
- [35] C. Wu and L. V. Zhigilei, Microscopic mechanisms of laser spallation and ablation of metal targets from large-scale molecular dynamics simulations, *Applied Physics A* **114**, 11 (2014).
- [36] E. Silaeva, A. Vella, N. Sevelin-Radiguet, G. Martel, B. Deconihout, and T. Itina, Ultrafast laser-triggered field ion emission from semiconductor tips, *New Journal of Physics* **14**, 113026 (2012).
- [37] M. Noda, S. A. Sato, Y. Hirokawa, M. Uemoto, T. Takeuchi, S. Yamada, A. Yamada, Y. Shinohara, M. Yamaguchi, K. Iida, I. Floss, T. Otobe, K.-M. Lee, K. Ishimura, T. Boku, G. F. Bertsch, K. Nobusada, and K. Yabana, Salmon: Scalable ab-initio light-matter simulator for optics and nanoscience, *Computer Physics Communications* **235**, 356 (2019).
- [38] K. Yabana, T. Sugiyama, Y. Shinohara, T. Otobe, and G. Bertsch, Time-dependent density functional theory for strong electromagnetic fields in crystalline solids, *Physical Review B* **85**, 045134 (2012).
- [39] A. D. Baczewski, L. Shulenburger, M. Desjarlais, S. Hansen, and R. Magyar, X-ray thomson scattering in warm dense matter without the chihara decomposition, *Physical review letters* **116**, 115004 (2016).
- [40] T. Otobe, Wavelength dependence of the laser-excitation process on a silicon surface, *Physical Review Applied* **13**, 024062 (2020).
- [41] K. Kaneshima, Y. Shinohara, K. Takeuchi, N. Ishii, K. Imasaka, T. Kaji, S. Ashihara, K. L. Ishikawa, and J. Itatani, Polarization-resolved study of high harmonics from bulk semiconductors, *Physical review letters* **120**, 243903 (2018).
- [42] H. Hirori, P. Xia, Y. Shinohara, T. Otobe, Y. Sanari, H. Tahara, N. Ishii, J. Itatani, K. L. Ishikawa, T. Aharen, M. Ozaki, A. Wakamiya, and Y. Kanemitsu, High-order harmonic generation from hybrid organic-inorganic perovskite thin films, *APL Materials* **7**, 041107 (2019).
- [43] Y. Sanari, H. Hirori, T. Aharen, H. Tahara, Y. Shinohara, K. L. Ishikawa, T. Otobe, P. Xia, N. Ishii, J. Itatani, S. A. Sato, and Y. Kanemitsu, Role of virtual band population for high harmonic generation in solids, *Physical Review B* **102**, 041125 (2020).
- [44] K. Ishikawa and T. Blenski, Particle-in-cell simulations of multiple ionization of small molecules in a strong laser field, *Physical Review A* **61**, 063408 (2000).
- [45] D. Palade and V. Baran, Optical response of c60 fullerene from a time dependent thomas fermi approach, *Journal of Physics B: Atomic, Molecular and Optical Physics* **48**, 185102 (2015).
- [46] E. Giglio, E. Suraud, and P.-G. Reinhard, Semi-classical description of ionic and electronic dynamics in metal clusters, *Annalen der Physik* **11**, 291 (2002).
- [47] T. Fennel, G. Bertsch, and K.-H. Meiwes-Broer, Ionization dynamics of simple metal clusters in intense fields by the thomas-fermi-vlasov method, *The European Physical Journal D-Atomic, Molecular, Optical and Plasma Physics* **29**, 367 (2004).
- [48] J. Köhn, R. Redmer, K.-H. Meiwes-Broer, and T. Fennel, Non-resonant absorption enhancement in laser-excited simple metal clusters through electron-electron collisions, *Physical Review A* **77**, 033202 (2008).
- [49] L. Plagne, J. Daligault, K. Yabana, T. Tazawa, Y. Abe, and C. Guet, Semiclassical versus quantal time-dependent mean-field descriptions of electron dynamics

- in ion-cluster collisions, *Physical Review A* **61**, 033201 (2000).
- [50] A. Doms, P.-G. Reinhard, and E. Suraud, Fermionic vlasov propagation for coulomb interacting systems, *annals of physics* **260**, 171 (1997).
  - [51] A. Doms, P. L'Eplattenier, P. Reinhard, and E. Suraud, The vlasov equation for coulomb systems and the husimi picture, *Annalen der Physik* **509**, 455 (1997).
  - [52] F. Calvayrac, P. Reinhard, and E. Suraud, Ionic structure and plasmon response in sodium clusters, *Journal of Physics B: Atomic, Molecular and Optical Physics* **31**, 1367 (1998).
  - [53] L. Féret, E. Suraud, F. Calvayrac, and P. Reinhard, On the electron dynamics in metal clusters: a vlasov approach, *Journal of Physics B: Atomic, Molecular and Optical Physics* **29**, 4477 (1996).
  - [54] Y. Abe, P. Bozek, and K. Yabana, Time-dependent local density approximation for cluster-ion collisions, *Czechoslovak journal of physics* **48**, 838 (1998).
  - [55] E. Runge and E. K. Gross, Density-functional theory for time-dependent systems, *Physical Review Letters* **52**, 997 (1984).
  - [56] E. P. Wigner, On the quantum correction for thermodynamic equilibrium, *Physical Review* **749**, 997 (1932).
  - [57] C. Fiolhais, J. P. Perdew, S. Q. Armster, J. M. MacLaren, and M. Bralczewska, Dominant density parameters and local pseudopotentials for simple metals, *Physical Review B* **51**, 14001 (1995).
  - [58] J. P. Perdew and A. Zunger, Self-interaction correction to density-functional approximations for many-electron systems, *Physical Review B* **23**, 5048 (1981).
  - [59] S. Tanaka, K. Yoshikawa, T. Minoshima, and N. Yoshida, Multidimensional vlasov–poisson simulations with high-order monotonicity-and positivity-preserving schemes, *The Astrophysical Journal* **849**, 76 (2017).
  - [60] G. F. Bertsch and S. D. Gupta, A guide to microscopic models for intermediate energy heavy ion collisions, *Physics Reports* **160**, 189 (1988).
  - [61] L. Verlet, Computer” experiments” on classical fluids. i. thermodynamical properties of lennard-jones molecules, *Physical review* **159**, 98 (1967).
  - [62] J. W. Cooley and J. W. Tukey, An algorithm for the machine calculation of complex fourier series, *Mathematics of computation* **19**, 297 (1965).
  - [63] G. F. Bertsch, J.-I. Iwata, A. Rubio, and K. Yabana, Real-space, real-time method for the dielectric function, *Physical Review B* **62**, 7998 (2000).
  - [64] K. Yabana and G. Bertsch, Time-dependent local-density approximation in real time, *Physical Review B* **54**, 4484 (1996).
  - [65] M. Fuchs and M. Scheffler, Ab initio pseudopotentials for electronic structure calculations of poly-atomic systems using density-functional theory, *Computer Physics Communications* **119**, 67 (1999).
  - [66] A. D. Rakić, Algorithm for the determination of intrinsic optical constants of metal films: application to aluminum, *Applied optics* **34**, 4755 (1995).
  - [67] T. Gharbi, D. Barchiesi, S. Kessentini, and R. Maâlej, Fitting optical properties of metals by drude-lorentz and partial-fraction models in the [0.5; 6] ev range, *Optical Materials Express* **10**, 1129 (2020).
  - [68] A. Kiselev, L. Akashev, and V. Kononenko, Effective electron mass in melts of aluminum, cerium, and al–3 at.% ce binary system., *Technical Physics* **49** (2004).
  - [69] A. Yamada and K. Yabana, Energy transfer from intense laser pulse to dielectrics in time-dependent density functional theory, *The European Physical Journal D* **73**, 1 (2019).
  - [70] M. Uemoto, S. Kurata, N. Kawaguchi, and K. Yabana, First-principles study of ultrafast and nonlinear optical properties of graphite thin films, *Physical Review B* **103**, 085433 (2021).